





Dynamic Control of Contractile Force in Engineered Heart Tissue

Huate Li, Subramanian Sundaram , Ruifeng Hu, Lihua Lou , Francisco Sanchez, William McDonald, Arvind Agarwal, Christopher S. Chen , and Thomas G. Bifano 

Abstract—Three-dimensional engineered heart tissues (EHTs) derived from human induced pluripotent stem cells (iPSCs) have become an important resource for both drug toxicity screening and research on heart disease. A key metric of EHT phenotype is the contractile (twitch) force with which the tissue spontaneously beats. It is well-known that cardiac muscle contractility – its ability to do mechanical work – depends on tissue prestrain (preload) and external resistance (afterload). **Objectives:** Here, we demonstrate a technique to control afterload while monitoring contractile force exerted by EHTs. **Methods:** We developed an apparatus that can regulate EHT boundary conditions using real-time feedback control. The system is comprised of a pair of piezoelectric actuators that can strain the scaffold and a microscope that can measure EHT force and length. Closed loop control allows dynamic regulation of effective EHT boundary stiffness. **Results:** When controlled to switch instantaneously from auxotonic to isometric boundary conditions, EHT twitch force immediately doubled. Changes in EHT twitch force as a function of effective boundary stiffness were characterized and compared to twitch force in auxotonic conditions. **Conclusion:** EHT contractility can be regulated dynamically through feedback control of effective boundary stiffness. **Significance:** The capacity to alter the mechanical boundary conditions of an engineered tissue dynamically offers a new way to probe tissue mechanics. This could be used to mimic afterload changes that occur naturally in disease, or to improve mechanical techniques for EHT maturation.

Index Terms—Biomedical imaging, cardiomyocyte, contractility, force control, tissue engineering.

Manuscript received 30 July 2022; revised 26 October 2022; accepted 21 January 2023. Date of publication 24 January 2023; date of current version 20 June 2023. The work of Subramanian Sundaram was supported by American Heart Association under Grant 20POST35210045. This work was supported by the National Science Foundation under NSF Cooperative through Engineering Research Centers Program under Grant EEC-1647837. (Corresponding author: Thomas G. Bifano.)

Huate Li, Ruifeng Hu, and Francisco Sanchez are with the Mechanical Engineering Department, Boston University, USA.

Subramanian Sundaram and Christopher S. Chen are with the Biomedical Engineering Department, Boston University, USA.

Lihua Lou and Arvind Agarwal are with the Department of Mechanical and Materials Engineering, Florida International University, USA.

William McDonald is with the Cambridge Rindge and Latin School, USA.

Thomas G. Bifano is with the Mechanical Engineering Department, Boston University, Boston, MA 02215 USA (e-mail: tgb@bu.edu).

Digital Object Identifier 10.1109/TBME.2023.3239594

I. INTRODUCTION

ENGINEERED heart tissues (EHTs) derived from human induced pluripotent stem cells (iPSCs) are used as *in vitro* models to study cardiac physiology [1], [2], [3]. One such engineered structure is the microfabricated tissue gauge (μ Tug), an elastomer scaffold comprised of a microwell with a pair of vertical compliant pillars extending upward from its base. The tops of the pillars serve as anchors for self-assembly of 3D EHTs that form over a period of days from a cell-laden gel of natural extracellular matrix materials [4]. An attribute of the cardiac μ Tug is that these tissue constructs, comprised of iPSC-derived cardiomyocytes and supporting cells such as fibroblasts or human mesenchymal stem cells (hMSCs), self-assemble to form spontaneously beating 3D structures that recapitulate some of the important physiology of cardiac muscle. When μ Tug EHTs are fully compacted, they begin periodic spontaneous contractions, or twitches. The resulting tensile force bends the pillar tops measurably toward one another. With a suitable imaging system and knowledge of pillar mechanical properties, one can infer EHT twitch force, a key functional metric for evaluating the performance of cardiac microtissues.

In addition to μ Tugs, 3D EHTs can be made using approaches that include cells molded in hydrogels and self-assembled tissues formed around biowire scaffolds. These approaches also allow suspension of the 3D EHT and optical monitoring of tissue contractile tension [5], [6].

Contraction dynamics of EHTs derived from iPSCs have been studied widely, and are characterized by parameters such as peak twitch tension, peak rate of change of tension for contraction and relaxation, and time from stimulus to peak tension [7]. These are sometimes used as surrogate measures of tissue maturation. A profound functional difference between EHTs derived from iPSCs and adult human cardiac muscle is the substantially larger contractility (ability to do mechanical work) of the latter.

The contractile behavior of these EHTs can be modulated by the mechanical stresses experienced during culture, not unlike native heart tissue. Pillars exert a linear elastic (i.e., auxotonic) external resistance, or *afterload*, in response to EHT generated forces. The stiffness of the pillars affects the magnitude of force generated by EHTs; stiffer pillars have been shown to increase twitch force and baseline tension [8]. Modulation of the stiffness of the matrix itself also is known to be essential in the process of cardiac tissue maturation. Driven by the accumulation of extracellular matrix materials like collagen, tissue stiffness increases

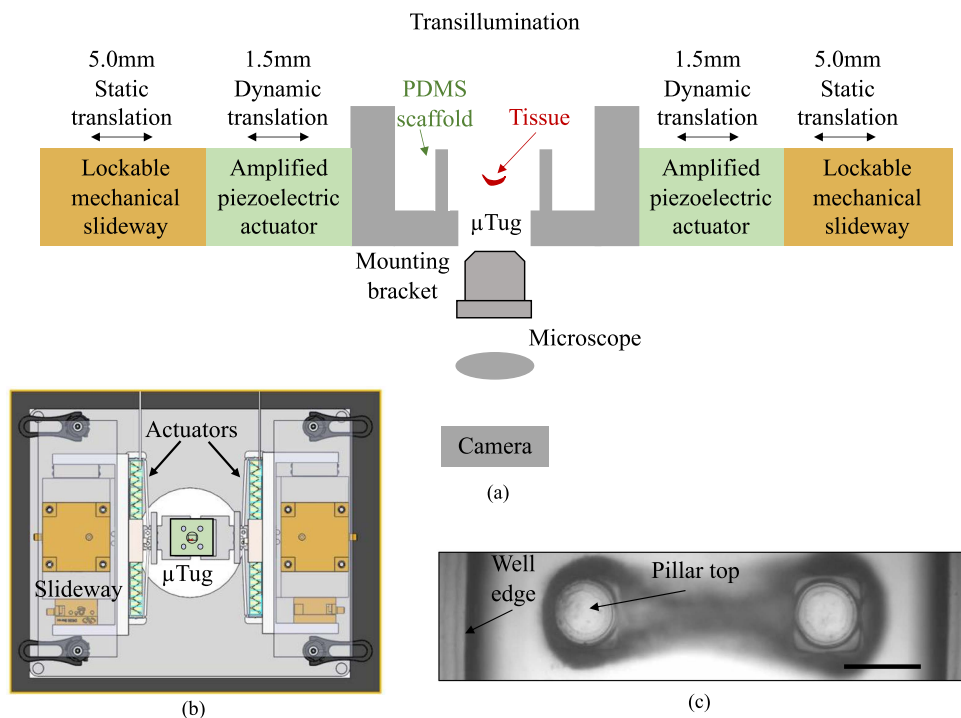


Fig. 1. Overview of the dynamic force control system. (a) Cross-sectional schematic depiction of the main actuation and measurement components. The EHT is supported by two PDMS pillars in a media-filled well at the center of a PDMS scaffold. The scaffold is supported by four prongs on a mounting bracket. The bracket is fixed to an amplified piezoelectric actuator that can impose dynamic tensile strain on the scaffold. A lockable mechanical slideway can be adjusted to impose static tensile strain on the scaffold. A transilluminated inverted microscope is focused on the scaffold pillar tops and well edges to monitor EHT force and scaffold strain. (b) Top view CAD schematic of the actuator and slideway assembly with a μ Tug scaffold. This assembly is maintained in an environmental chamber that regulates temperature, humidity, and carbon dioxide concentration. (c) Microscope image of the scaffold with an EHT. Pillar tops and well edges are in sharp focus. Actuation is in the horizontal direction and produces axial strain of the scaffold resulting in changes in EHT force and length. Scale bar: 1 mm.

severalfold from embryonic to adult stage [9]. In addition to the effects of passive mechanical conditions, forces actively applied to the EHTs can precondition them mechanically through quasistatic stretching, known as *preload*. Preconditioning has been shown to increase EHT maturity and to increase twitch force [10]. Several previously reported studies of EHTs use scaffolds that allow some dynamic mechanical control of EHT force or length using electromagnetic, pneumatic, or piezoelectric [11], [12], [13], [14] actuation. Some have incorporated dynamic force control to regulate and measure tissue tension simultaneously [15], [16], [17].

In this work we aim to study the effect of afterload on tissue contractility by monitoring EHT twitch forces in a scaffold that can be controlled dynamically to alter the external resistance (i.e., stiffness) of scaffold pillars that support the EHT. The extremes for such mechanical scaffold constraints are isometric (perfectly rigid pillars) and isotonic (perfectly compliant pillars). Without control, pillars provide auxotonic boundary conditions that fall somewhere between those extremes.

We developed a real-time force feedback control system that regulates afterload and monitors its effect on EHT twitch force. Effective pillar stiffness is maintained through closed-loop control of a pair of mechanically amplified piezoelectric actuators that can stretch or compress the scaffold rapidly in response to measured changes in EHT force or length. The system employs a high-speed CMOS camera integrated with an inverted widefield

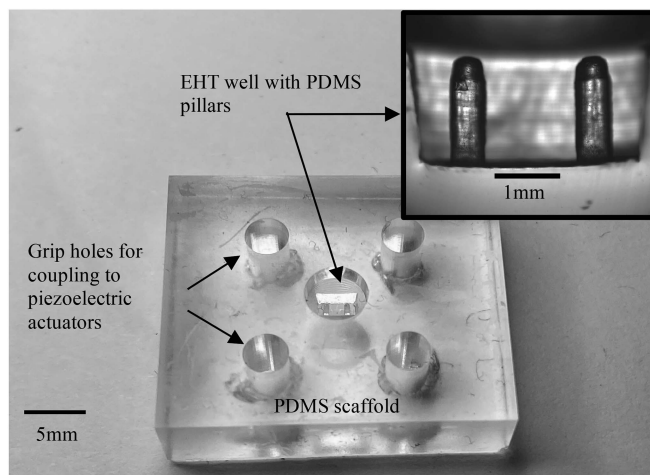


Fig. 2. Photo of the PDMS scaffold, fabricated using direct molding from a 3D printed template. Inset shows a magnified side view of the pillars in the nutrient media well.

microscope to monitor pillar deformation and scaffold strain, from which EHT contractile force can be inferred. A simple schematic of the system is depicted in Fig. 1.

An image of the molded polydimethylsiloxane (PDMS) scaffold used in this system is shown in Fig. 2. The structure measures 5 mm tall, 25 mm deep, and 20 mm wide. It features

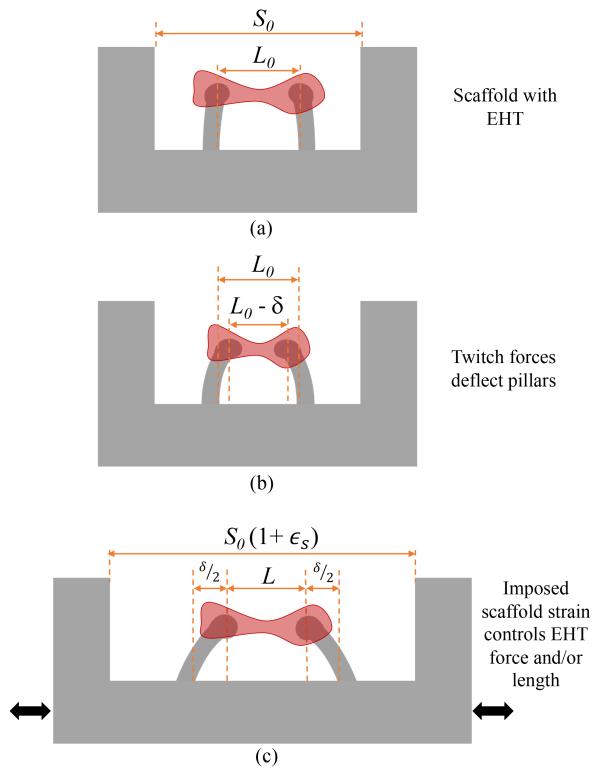


Fig. 3. Cross sectional schematic of the EHT, pillars, and nutrient well to illustrate basic system function. (a) Cardiomyocytes derived from iPSCs and supporting cells form a compacted EHT spanning the scaffold pillars. Static tension exerted by the EHT deflects the pillar tops toward one another. The initial EHT length is L_0 and the initial well length is S_0 . (b) Without control, spontaneous periodic EHT contraction (i.e., twitch force) deflects pillar tops toward one another by an amount δ . Assuming linear elastic pillars, EHT twitch force F_p can be estimated as $k_p \delta$, where k_p is the pillars' combined stiffness. (c) During control, the actuators strain the scaffold by an amount ϵ_s to achieve a control objective for measured EHT length or force. As an example, for isometric control the objective would be to keep pillar tops always separated by a distance L_0 , counteracting any change of EHT length in response to twitch forces.

two pairs of grip holes spaced 10 mm apart to the left and right of the EHT well that align with prongs on a mounting bracket. Pillars are square in cross section, $450 \mu\text{m}$ wide and $1450 \mu\text{m}$ tall, converging to a spherical cap. Pillar separation is $1580 \mu\text{m}$.

System operation is illustrated schematically in Fig. 3. Scaffold strain imposed by the actuators is measured by tracking separation of the edges of the nutrient well. EHT length is measured by tracking the separation of pillar tops. Actuation stretches the scaffold, allowing control of tissue length or force.

The control system is capable of subjecting EHTs to boundary constraints that are effectively stiffer or more compliant than the pillars would be without control.

II. MATERIALS AND METHODS

A. Elastomeric Scaffold and EHT Preparation

The molds for generating the elastomeric scaffolds were designed using CAD tools (Solidworks) and 3D-printed with the MicroFineTM Green resin by Stereolithography (Protolabs, Maple Plain, MN, USA). The printed parts received were rinsed

in ethanol and then blown dry with an air gun. After cleaning, PDMS scaffolds were made using these molds with a 20:1 mixture of monomer to crosslinker (Sylgard 184 Silicone Elastomer Kit), and cured overnight at 60°C . After demolding, the PDMS parts were further cured overnight at 100°C in a convection oven.

Prior to cell seeding, PDMS scaffolds were plasma treated (EMS 1050x, Quorum Technologies) for 30 s followed by a 2 h treatment in 0.01% poly-L-lysine (PLL) and 1% glutaraldehyde (Electron Microscopy Sciences, Inc) for 10min. These treatments help the EHT adhere to the PDMS pillars. The scaffolds were rinsed three times in phosphate buffered saline and left to sit at 4°C for two nights in DI water. The PDMS scaffolds were then soaked in 100% ethanol for 15min, dried and UV sterilized for 15min. The devices were transferred to a tissue culture hood and the bottom portion of the rectangular well was treated with 2% Pluronic F-127 for 30min to prevent adhesion of the EHT to the bottom surface of the rectangular well.

The cardiomyocytes used here under Boston University IRB Protocol 1820, approved February 2020, were generated from iPSCs using the PGPI parent line (white adult male, born 1954), and differentiated by temporal modulation of regulators of the Wnt signaling pathway [18]. After differentiation, the hiPSC-derived CMs were purified by lactate starvation for 4 days (glucose free RPMI with 4 mM sodium lactate). Once purified, the iPSC-CMs were transferred to fresh fibronectin treated plates and maintained in RPMI containing B-27 Supplement (1:50 dilution) for up to a month. Tissue culture plates were treated with $10 \mu\text{g/ml}$ fibronectin (Corning 356009; Fischer Scientific) overnight at 4°C . A mixture of 90% iPSC-CMs and 10% hMSCs totaling ~ 60000 cells and suspended in 5.5 μL of extracellular matrix (ECM) mixture containing 4 mg/ml fibrin (human fibrinogen, MilliporeSigma with 0.4 U/mg thrombin, MilliporeSigma) and 10% Matrigel (Corning) was added to each PDMS well. The PDMS scaffolds were placed upside down to allow the cells to settle close to the top of the pillars during polymerization.

After crosslinking ($\sim 5\text{min}$), the cell-laden hydrogel was cultured in growth media made with high-glucose DMEM containing 10% fetal bovine serum (MilliporeSigma), 1% penicillin-streptomycin, 1% nonessential amino acids (Fisher) and 1% GlutaMAX (Fisher) supplemented with $5 \mu\text{M}$ Y-27632 and $33 \mu\text{g/ml}$ aprotinin. About $50 \mu\text{L}$ of growth media was added to each PDMS device containing the cell-laden hydrogel and stored in an incubator at 37°C with 5% CO_2 . The ROCK inhibitor Y-27632 was removed after 1 day of culture and the media was replaced every two days. Over the course of 2-5 days, the cell-laden media gradually compacts to form the EHT.

B. μTug Microscope Force Control System

The scaffold is manually inserted into the force control system by aligning holes in the scaffold with prongs protruding from the mounting basket. The bracket is attached rigidly to one side of a mechanically amplified piezoelectric actuator (APF710, Thorlabs). The opposing side of the actuator is mounted to a lockable ball-bearing linear slideway that is fixed to a rigid

base plate. The slideway can be adjusted to impose up to 50% static tensile strain to the scaffold. However, for all experiments reported in this work, that slideway was adjusted to produce 0% initial static scaffold strain.

The actuators are controlled using a data acquisition module (PCI6251, National Instruments) and a multichannel high voltage piezoelectric actuator driver (MDT693B, Thorlabs). The piezoelectric actuators have a nominal resonant frequency of 185Hz. The pair of actuators combine to allow a full range of motion of 3 mm with a resolution of ~ 50 nm and can provide up to 14% dynamic strain to the scaffold.

The transilluminated microscope (IX73, Olympus) uses a 2.5X (0.08NA) objective lens (MPLFN2.5X, Olympus) and a fast CMOS camera (PCO Edge4.2, PCO AG) to image the EHT in real time. The microscope resolution is $4.19 \mu\text{m}$ and the camera slightly oversamples this with image resolution of $2.95 \mu\text{m}$ per pixel. The imaging field of view can be as large as $6.0 \text{ mm} \times 6.0 \text{ mm}$ for initial setup and alignment. To allow faster acquisition during control, the field of view is truncated to $6.0 \text{ mm} \times 96 \mu\text{m}$.

The base plate, actuators, and scaffold are enclosed in a custom-built environmental enclosure that regulates temperature, humidity, and carbon dioxide concentration at set points of 37°C , 50%, and 5% respectively.

C. Force and Effective Stiffness Measurement

Before control, the μTug with EHT is mounted to the actuator mounting plate at a condition of 0% scaffold strain. The microscope is adjusted to center the image of pillars in the field of view and to focus on the pillar tops and well edges. An initial reference image of the pillars and well edges is acquired.

The closed-loop force control system cycle time is ~ 3.2 ms, corresponding to a 313 Hz image acquisition frame rate. In each cycle, the camera acquires an image of the pillar tops and the well edges. Four selected subregions of the image corresponding to the pillar tops and the well edges are cross correlated with corresponding subregions of the reference image using an intrinsic MATLAB image cross correlation function to estimate changes in scaffold well edge separation and pillar top separation. As expected, localization is more precise than nominal image resolution. The typical noise floor for localization, given the selected imaging system and image correlation algorithms, is $\sim 0.25 \mu\text{m}$.

The two system variables that are readily measured from cross-correlated images are EHT length, L , defined by the lateral separation of pillar tops, and scaffold strain, ϵ_s defined as the change in lateral separation of the scaffold well edges divided by the initial (unstrained) lateral separation of the scaffold well edges.

The instantaneous EHT force is the product of pillar deflection and the stiffness the pillars in the direction of the applied force:

$$F_p = \delta k_p \quad (1)$$

Because the scaffold material is linearly elastic, stiffness is constant. Pillar deflection is due to a combination of bending, shear, and distortion of the pillar's attachment to the scaffold

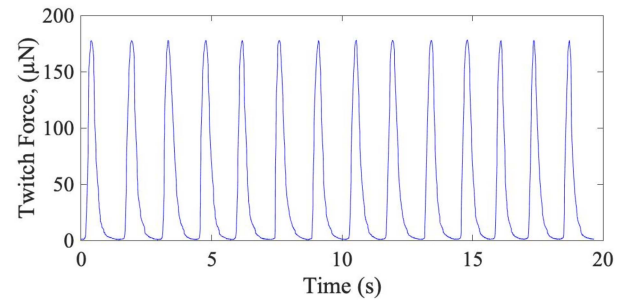


Fig. 4. Measured EHT force for a typical μTug sample. The frequency of spontaneous contractions is ~ 0.68 Hz, and the average twitch force is $177 \mu\text{N}$.

base. EHT length, or, equivalently, pillar top separation, L can be affected by both EHT-induced pillar deflection and actuator-induced scaffold strain. We separate these two components by measuring, as a baseline, pillar top separation as a function of imposed scaffold strain when there is no EHT in the scaffold and fitting it to a linear equation:

$$L_b = a\epsilon_s + b \quad (2)$$

where a and b are the coefficients of a least squares linear fit to the measured data. Thereafter, pillar deflection δ can be inferred as the difference between the measured pillar top separation L and the baseline pillar top separation L_b associated with the current scaffold strain ϵ_s .

For each batch of scaffolds used to make EHT samples, one scaffold was destructively tested to measure pillar lateral stiffness directly using an *in-situ* indenter for soft biomaterials (Hysitron Biosoft, Bruker). Sample scaffolds were trimmed and mounted on glass slides to expose individual pillars to the indenter. The indentation test included first contacting the top of a pillar, then applying $100 \mu\text{m}$ of lateral displacement at $5 \mu\text{m/s}$ loading rate, followed by unloading at the same rate. From the slope of the nominally linear unloading curve the stiffness of the pillars could be calculated directly. We found that the lateral stiffness for the pillars used in our scaffolds was $2.88 \pm 0.45 \text{ N/m}$. Based on this measured stiffness and the noise floor of the cross-correlated localization measurements of pillar deflection, we estimate the EHT contractile force measurement noise floor to be $\sim 0.72 \mu\text{N}$.

Fig. 4 is a plot of measured force as a function of time over a twenty second period for a typical EHT with no applied scaffold strain and no control. The average EHT twitch force, measured from peak to baseline, is $177 \mu\text{N}$.

We measure forces and strains of the EHT relative to the reference state of the EHT at rest in the unstrained scaffold (i.e., at length L_0). Of course, the internal strain of the suspended EHT is not zero in this reference state, nor is its tensile force zero. Even in an unstrained scaffold, the compacted EHT exerts a tensile force on the pillars. More commonly in the literature, the reference condition associated with zero internal strain and zero tensile force is when the EHT is released from load-bearing constraints. Empirically, we have observed (by releasing one end of an EHT from the μTug) that in this zero-strain reference state the EHT nominal length is approximately, suggesting a tensile

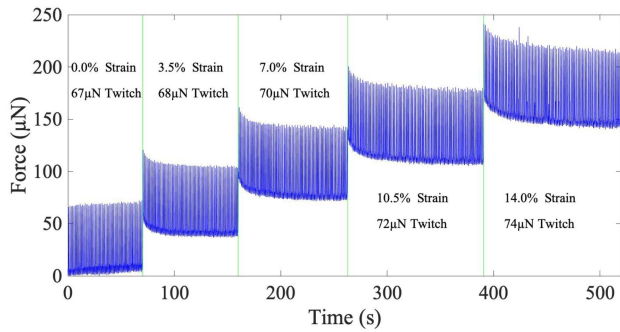


Fig. 5. Top: Measured EHT forces for applied scaffold strains varying in five steps from 0% to 14% over a 520 second test. In each zone, the scaffold strain was maintained at a constant value through feedback control and more than 50 spontaneous contractions were recorded. Average twitch force is shown for each stress state.

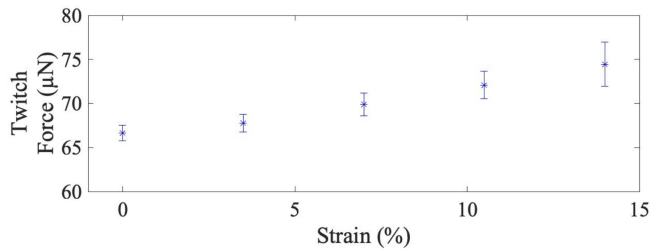


Fig. 6. Average twitch force as a function of scaffold strain, derived from the data in Fig. 5. The EHT exhibited 10% increase in twitch force in response to a 14% increase in tensile strain. Error bars correspond to measurement standard deviation.

strain of $\sim 100\%$ for the EHTs in their compacted initial state on the μ Tug. Since this reference state is generally inaccessible in our system (EHT removal from the scaffold is irreversible), we instead chose to reference EHT force and length from baseline measurements in the unstrained scaffold.

It is well-known that EHTs exhibit a Frank-Starling mechanism: The amplitude of twitch force increases with increasing EHT length, approaching an asymptotic limit [19]. Since our apparatus achieves contractile force control through strain of the scaffold (and consequently, changes in length of the EHT), it is important that we evaluate the scale of the Frank Starling effect over the range of strains to be used in control.

Fig. 5 depicts a measurement of EHT forces recorded for five scaffold strain conditions that correspond to the full displacement range achievable with our piezoelectric actuation system. Each scaffold strain condition was maintained using feedback control to prevent changes in scaffold strain that would otherwise occur due to actuator creep and hysteresis. The results show a 10% increase in twitch force magnitude, from $67\mu\text{N}$ to $74\mu\text{N}$, in response to a 14% increase in scaffold strain, indicative of a Frank Starling effect that is near its plateau, as depicted in Fig. 6. Over the span of this test the EHT lengthened by $112\mu\text{m}$ (7%) and the baseline EHT force increased by $149\mu\text{N}$. This Frank Starling effect is consistent with what others have reported with similar EHT configurations [20]. Also apparent in Fig. 5 is a viscoelastic relaxation of the EHT that occurs after each step increase in scaffold strain, with a first-order decay and

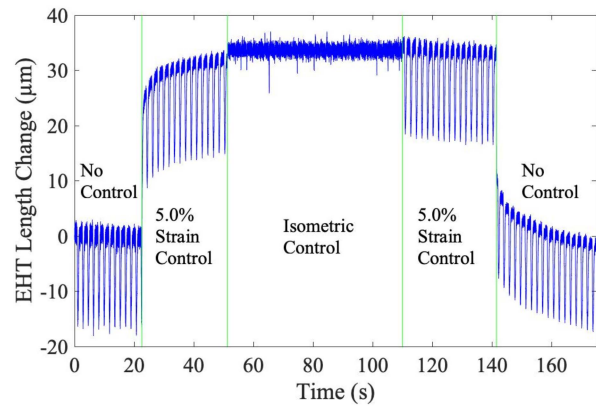


Fig. 7. EHT length change during isometric closed loop control, with the control objective to hold the EHT at fixed length irrespective of contractile force.

a relaxation time constant of about 15 seconds. This effect is well-documented for EHTs subjected to externally applied rapid stretching [21].

The instantaneous *effective* pillar stiffness, k_{eff} , of the boundary attachments from the perspective of the EHT can be defined as the force on the pillars divided by the change in EHT length (which is equivalent to the change in pillar top separation, $L - L_0$):

$$k_{eff} = \frac{F_p}{(L - L_0)} \quad (3)$$

where L_0 is the reference EHT length measured when the scaffold is unstrained, and L is the instantaneously measured EHT length. Note that if the scaffold strain is held at zero (i.e., no actuation), then $\delta = L - L_0$, leading (from (1)) to the auxotonic boundary condition $k_{eff} = k_p$ as expected.

To make the effective stiffness as large as possible, the control objective would be to maintain constant EHT length: $L = L_0$. A more general control strategy to achieve an arbitrary effective stiffness ratio k_{eff}/k_p is found by combining (1) and (3):

$$\frac{k_{eff}}{k_p} = \frac{\delta}{L - L_0} \quad (4)$$

leading to a control objective to maintain a fixed ratio of pillar deflection to changes in EHT length.

D. Feedback Control System

Integral feedback control was used to maintain the specified control objectives for afterload control experiments. More complex control approaches, including those with proportional and derivative feedback and those with feedforward compensation might improve controller performance. Active electrical pacing of the EHT might also improve controller performance by making the onset of contractile forces more predictable temporally.

To determine if the measured system closed loop control bandwidth is adequate to regulate force in a spontaneously contracting EHT, we first estimated the amplitude spectrum of the time series of recorded spontaneous twitch contractions over a bandwidth of ~ 156 Hz (the Nyquist limit for our 313 Hz image

acquisition rate). The measured power is indistinguishable from noise at frequencies above 15 Hz. Next, we evaluated the control system's closed-loop frequency response in an experiment implemented on a scaffold without tissue. The control objective was to produce an instantaneous small step change in the scaffold strain (2.5%) corresponding to about one fifth of the achievable control range, as quickly as possible using integral feedback control. Strain response of the scaffold was recorded in real time. The time constant associated with the strain step response was found to be 0.0144 ± 0.0024 s. This implies a small signal bandwidth of ~ 69 Hz for the closed-loop control system, fast enough to control essentially all measurable dynamics associated with typical spontaneous EHTs twitch forces.

III. RESULTS

A. Isometric Control

We first used feedback control to enforce isometric boundary conditions for the EHT. In these experiments, the measured spontaneous twitch force under isometric control was found to increase in comparison to the measured spontaneous twitch force under auxotonic conditions for the same EHT.

Since the force control system uses pillar displacement as its feedback signal, some deflection of that pillar must occur before the actuators can counteract pillar motion. Hence, when implementing isometric control, the boundary stiffness is not infinite but is limited by the increment of pillar deflection required to generate a feedback signal. We can measure the effective stiffness as the ratio of the measured EHT force to the corresponding pillar deflection. Under closed loop isometric control we estimate the effective stiffness of the scaffold to be about 45 N/m, or 15 times stiffer than without control.

Closed-loop control experiments were performed on EHTs with a control objective to maintain isometric boundary conditions dynamically for tissues. The EHT was subject to closed loop control for about a minute in each experiment,

Fig. 7 illustrates in a typical experimental result showing the effectiveness of the control algorithm in maintaining fixed EHT length despite spontaneous contractile force perturbations. The results are plotted in five zones corresponding to the stages of control. In the first zone (0–26 s), the scaffold nominal strain is 0% and actuators are unenergized. In the second zone (26–52 s) the controller maintains scaffold strain at 5%. In this stage the EHT gradually relaxes, increasing its baseline length by $7 \mu\text{m}$ (0.4% of the nominal EHT length). The purpose of imposing this 5% scaffold strain is to position the piezoelectric actuator in a region of its control range that will allow it to impose both positive and negative scaffold strain in the following zone (isometric control). In the third zone (52–109 s), the isometric controller maintains constant EHT length at a level corresponding to the reference EHT length measured just prior to isometric control initiation. We note that there is a $2 \mu\text{m}$ increase in EHT length (0.1% of the nominal EHT length) at the transition to control that is likely due to an error in measurement of the reference EHT length just prior to control. In the fourth zone, (109–141 s) the controller maintains scaffold strain at 5%. In the final zone (141–175 s), the controller is turned off and the piezoelectric

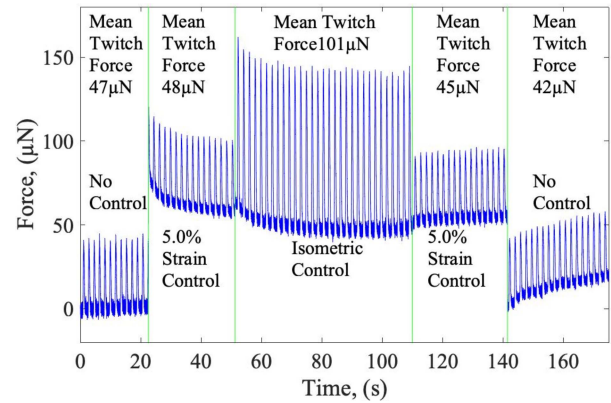


Fig. 8. EHT force measured during the isometric control experiment depicted in the previous Figure. The magnitude of spontaneous twitch force increases by a factor of 2.11, from $48 \mu\text{N}$ to $101 \mu\text{N}$, upon initiation of isometric boundary control.

actuators are unenergized. Because there is no control, the drift in the EHT length in this zone can be due to both tissue relaxation and actuator creep.

Fig. 8 is a plot of EHT force corresponding to the experimental result depicted in Fig. 7. Prior to control, the EHT auxotonic twitch force was measured to be about $48 \mu\text{N}$. When subjected to isometric boundary control, the EHT twitch force immediately increased to $101 \mu\text{N}$, more than twice as large as it was just prior to control. Upon cessation of isometric control, the twitch force immediately returned to $45 \mu\text{N}$, slightly lower than it was prior to isometric control.

We define the *normalized twitch force* as the average twitch force magnitude during control (zone 3) divided by the average twitch force magnitude under auxotonic conditions (zone 2). For the data shown in Figs. 7 and 8, the normalized twitch force for isometric control was 2.11.

We conducted 43 repetitions of this isometric control test on a total of 21 different EHT replicates. The EHT replicate average isometric twitch force was 2.14 ± 0.42 times larger than the auxotonic twitch force. This relative increase in twitch force was found to be independent of auxotonic twitch force magnitude, which ranged from $12 \mu\text{N}$ to $230 \mu\text{N}$ with a mean of $70 \mu\text{N}$ for the EHTs used in this series of experiments.

The ratio of isometric twitch force to auxotonic twitch force for isometric control will depend on the native auxotonic stiffness of the scaffold. Scaffolds that have higher auxotonic stiffness (for example, those made using a formulation of PDMS made with a lower ratio of monomer to crosslinker), should exhibit a smaller ratio of isometric twitch force to auxotonic twitch force since their auxotonic stiffness is closer to isometric. To verify this, we made μTug scaffolds with a 10:1 mixture of PDMS monomer to crosslinker, which is known to increase the modulus of elasticity of the polymer in comparison to the 20:1 mixture of monomer to crosslinker used to fabricate scaffolds for our initial experiments. We measured the stiffness of these pillars to be $4.82 \pm 0.013\text{N/m}$, about 67% stiffer than the scaffolds used in our initial experiments. We conducted an additional 49 repetitions of this isometric control experiment on a total of 12 different EHT replicates with the stiffer scaffolds. The

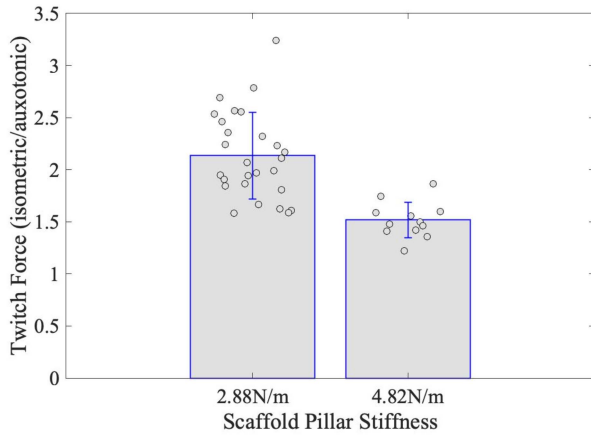


Fig. 9. EHT twitch force increase measured for two different auxotonic pillar stiffnesses. For 21 tissue replicates on pillars with 2.88 N/m stiffness, isometric boundary control led to an average twitch force that was 2.14 times that of the auxotonic twitch force. For 12 tissue replicates on pillars with 4.82 N/m stiffness, isometric boundary control led to an average twitch force that was 1.52 times the auxotonic twitch force. Error bars correspond to measurement standard deviation. Unpaired t-test $p < 0.00002$.

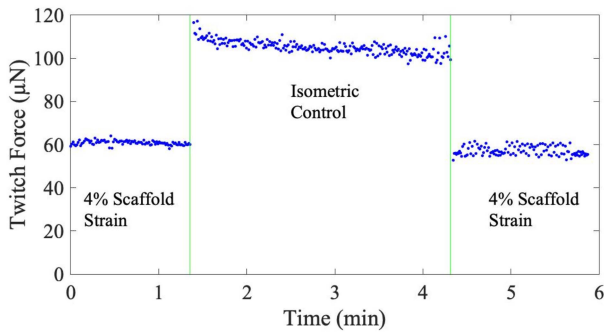


Fig. 10. Results from a longer-term isometric control experiment in which control was maintained for three minutes while monitoring twitch forces on an EHT. During isometric control the twitch force increased by a factor of 1.93.

EHT replicate average isometric twitch force was 1.52 ± 0.17 times larger than the auxotonic twitch force. As expected, the normalized isometric twitch force measured for EHTs in stiffer scaffolds is lower than that measured for EHTs in more compliant scaffolds. The results of all isometric control experiments, inclusive EHTs with both scaffold types, are shown in Fig. 9.

In an extended-duration experiment, we maintained isometric control for a duration of three minutes for an EHT in a scaffold with 2.88 N/m pillar stiffness. Before and after isometric control the scaffold was maintained at 4% strain. The isometrically controlled twitch force increased immediately with respect to the pre-control twitch force by a factor of 1.93 (from $60 \mu\text{N}$ to $116 \mu\text{N}$). Over the course of the three-minutes of continuous isometric control, the twitch force declined by about 10%, which could be attributed to viscoelastic relaxation. After control was stopped, the twitch force returned to a mean level of $57 \mu\text{N}$, $\sim 5\%$ lower than its mean value before isometric control. The results are illustrated in Fig. 10.

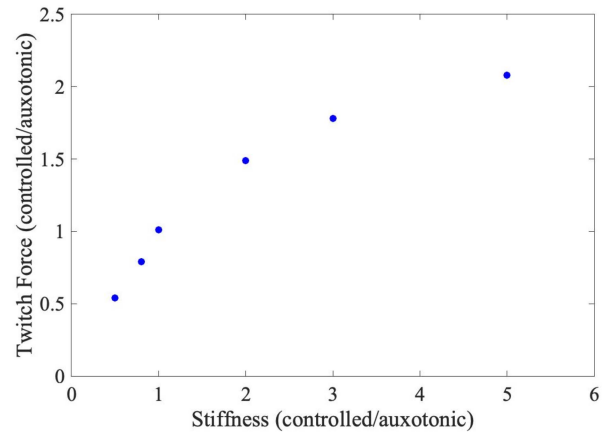


Fig. 11. Plot of the measured twitch forces (normalized by auxotonic twitch force) for a single EHT subjected to stiffness control corresponding to six different effective stiffnesses ranging from 0.5 to 5.0 times the scaffold auxotonic stiffness. Each data point corresponds to a single experiment comparable to those shown in Figs. 7 and 8 but using a control objective to maintain a specific stiffness ratio (k_p/k_{eff}) rather than to maintain isometric conditions.

B. Effective Stiffness Control

To further study the relationship between EHT twitch force and scaffold boundary stiffness, we conducted experiments with a control objective to maintain a desired *effective stiffness ratio* k_{eff}/k_p , as defined in (4). We can impose either stiffer or more compliant boundary conditions than the auxotonic (i.e., uncontrolled) boundary conditions for the EHT, limited primarily by the range of motion and dynamics of the piezoelectric actuators. In practice, we can reliably control scaffold effective stiffness to any value from 1.5 N/m to 45 N/m. Consequently, for our pillars with auxotonic stiffness measured to be 2.88 N/m, the achievable range of *effective stiffness ratios*, would be ~ 0.52 to 15.6.

We conducted a series of effective stiffness control experiments on EHTs. For a typical EHT, Fig. 11 shows the twitch force measured during control, normalized by the auxotonic twitch force measured just prior to control, as a function of the stiffness ratio. As expected, for an effective stiffness of 1, the normalized twitch force is also 1. For controlled stiffness greater than the auxotonic stiffness, the normalized twitch force increases nonlinearly toward an asymptote at higher relative stiffnesses. An *isometric* control experiment on this EHT yielded an isometric increase in twitch force ratio by a factor of 2.46. As expected, for controlled stiffness ratios smaller than 1 (i.e., controlled stiffness lower than that of the auxotonic pillars) the normalized twitch force was lower than 1.

Fig. 12. shows the ensemble results from 42 experiments on 9 different EHT biological replicates, with at least 4 EHTs tested at each effective stiffness ratio. The error bars correspond to one standard deviation for the EHT replicate data at each stiffness ratio. Measurement errors increase at high values of k_{eff}/k_p due to the smaller pillar deflection measurements that comprise the error signal used in control feedback. Again, the relative twitch force increases toward an asymptotic limit at higher stiffness ratios.

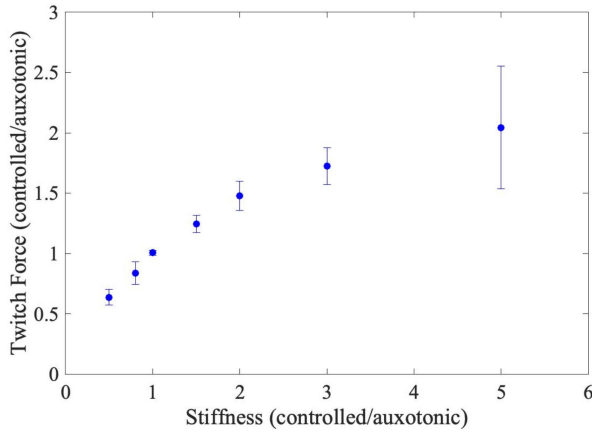


Fig. 12. Ratio of controlled twitch force to auxotonic twitch force for an ensemble of effective stiffness control experiments. Each data point corresponds to at least four tests conducted at a particular ratio of controlled pillar stiffness to auxotonic pillar stiffness, ranging from 0.5-5.0. Error bars correspond to measurement standard deviation.

Errors in pillar lateral stiffness measurements that are used in force calculation affect both controlled and auxotonic twitch force measurements proportionally, so those errors will not affect the normalized twitch force. Since only pillar top separation and well separation are measured during control, systematic errors in the calibration that links baseline pillar separation to imposed scaffold strain (as previously described in Section II-C.) could affect the calculated twitch force during control. We conducted an experiment to try to evaluate this potential source of error. We actuated scaffolds with no EHT over the full scaffold strain range while inferring contractile force from pillar top separation and well separation measurements. The inferred pillar bending force *should* remain zero in this case since there is no tissue to exert a load. We found that the inferred force remained below $10 \mu\text{N}$ for the entire range of scaffold strain.

C. Control After Treatment With Isoproterenol

The system described here can be used to control scaffold stiffness for EHTs treated with drugs that are known to alter EHT twitch force dynamics and to increase beat frequency. We conducted isometric control experiments on 18 EHT replicates that were subjected to isometric control, then treated with a $10 \mu\text{M}$ solution of isoproterenol and allowed to stabilize for thirty minutes before subjecting them to isometric control a second time. Isoproterenol is known to have a small effect on twitch force in EHTs, but a big effect on beat frequency and rate of change of twitch force during contraction [22].

Prior to isoproterenol treatment, the EHT replicates had a baseline beat frequency that averaged 1.00 ± 0.35 Hz. Isoproterenol treatment resulted in an increase in average EHT replicate beat frequency of 29%, as depicted in Fig. 13. We observed no statistically significant increase in twitch force. Peak twitch contraction rate (i.e., the maximum rate of change of twitch force as a function of time during EHT contraction) generally increased after isoproterenol treatment, by up to 206%. Fig. 14 is a plot of the (uncontrolled) twitch profile of the

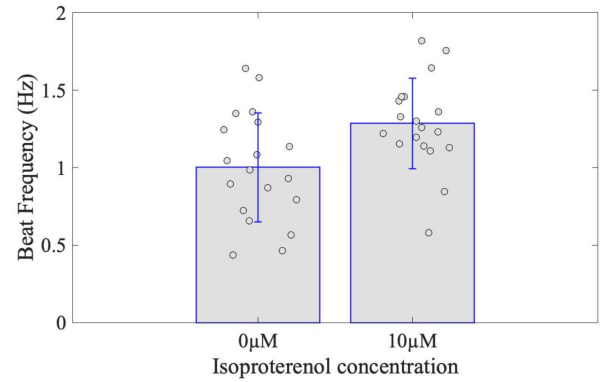


Fig. 13. EHT exposure to $10 \mu\text{M}$ isoproterenol resulted in 29% higher beat frequency, when averaged for the 18 EHT replicates. Error bars correspond to measurement standard deviation. Paired t-test $p < 0.0002$.

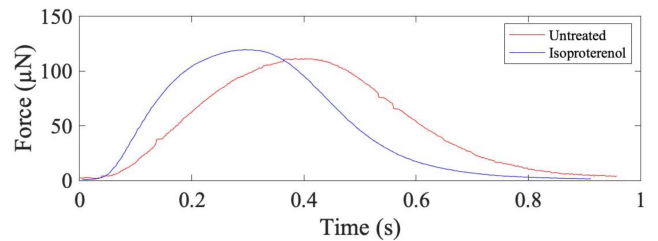


Fig. 14. After exposure to $10 \mu\text{M}$ isoproterenol, the auxotonic twitch force peak contraction rate (steepest slope of the rising twitch force) was about twice as large as the baseline value in the EHT for which this parameter changed most substantially.

EHT with the most significant change in contraction rate (from $470 \mu\text{N/s}$ to $967 \mu\text{N/s}$) after isoproterenol treatment.

The increased rate of contraction places more demand on the closed-loop controller by increasing the speed at which changing forces must be compensated. However, the controller has more than enough closed loop bandwidth to manage this more rapid twitch force dynamic. Consequently, the observed increases in beat frequency and peak contraction rate did not adversely affect the system's closed-loop performance during isometric boundary control. Measured values of normalized twitch force increase during isometric control were comparable to those measured before isoproterenol treatment (Fig. 15).

IV. DISCUSSION

The results point to a strong correlation between controlled boundary stiffness and twitch force in EHTs. The twitch force increases immediately when subjected to stiffer boundary conditions. The ratio of controlled twitch force to auxotonic twitch force increases asymptotically with increases in controlled boundary stiffness, approaching a value that depends on the scaffold's auxotonic stiffness. This effect is both instantaneous and independent of the auxotonic twitch force magnitude of EHTs.

EHT boundary stiffness has been shown to affect maturation of EHTs [8]. The capacity to control this boundary stiffness

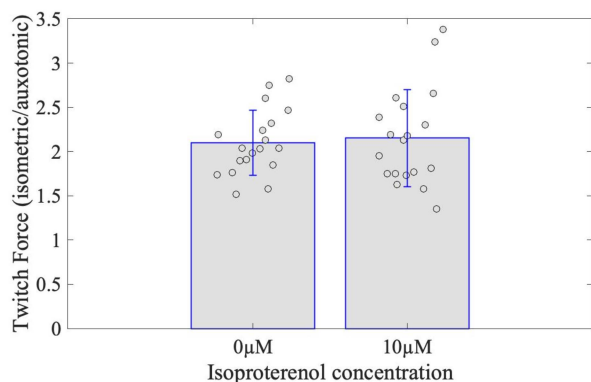


Fig. 15. Exposure to isoproterenol was not found to have a statistically significant effect on twitch force. The normalized increase in twitch force during isometric control of EHTs exposed to 10 μM isoproterenol was within 1.25% of the normalized increase in twitch force before exposure, when averaged for the 18 EHT replicates. Paired t-test $p > 0.6$.

dynamically and to alter it over time could allow more detailed studies concerning the effect of time-varying boundary constraints on tissue development and maturation.

Mechanical conditions, such as afterload, preload, stiffness, and stretching, can influence cardiac tissues not only in healthy but also pathological states including in hypertrophy [23].

Our platform allows one to program a time varying afterload through effective stiffness control. We can use the platform to characterize changes to contractile function (including characterization of the Frank-Starling relationship) that might occur during the onset, progression, or resolution of various cardiovascular disease settings. Moreover, because our platform allows one to program a time varying afterload, one can also mimic the natural dynamics of different physiologic and pathologic afterloads and examine whether exposure to such loading conditions can themselves alter tissue biology and function.

V. CONCLUSION

We have described a novel EHT force control system that has the capacity to alter afterload of EHTs and to regulate scaffold stiffness through direct force feedback. The imposition of more rigid boundary constraints on EHTs has been shown to instantaneously increase the contractile force exerted by the EHT. The dependence of twitch force on EHTs subjected to boundary stiffnesses above and below the auxotonic stiffness has been characterized.

ACKNOWLEDGMENT

The authors would like to thank Paige Cloonan and Joshua Lee for assistance with culturing EHTs and Marva Lawrence for assistance with scaffold stiffness measurement.

REFERENCES

- [1] G. Camprotrini et al., "Cardiac tissues from stem cells: New routes to maturation and cardiac regeneration," *Circulation Res.*, vol. 128, no. 6, pp. 775–801, Mar. 2021, doi: [10.1161/circresaha.121.318183](https://doi.org/10.1161/circresaha.121.318183).
- [2] J. T. Hinson et al., "Titin mutations in iPSC cells define sarcomere insufficiency as a cause of dilated cardiomyopathy," *Science*, vol. 349, no. 6251, pp. 982–986, 2015, doi: [10.1126/science.aaa5458](https://doi.org/10.1126/science.aaa5458).
- [3] B. M. Ogle et al., "Distilling complexity to advance cardiac tissue engineering," *Sci. Trans. Med.*, vol. 8, no. 342, Jun. 2016, Art. no. 342ps13, doi: [10.1126/scitranslmed.aad2304](https://doi.org/10.1126/scitranslmed.aad2304).
- [4] W. R. Legant et al., "Microfabricated tissue gauges to measure and manipulate forces from 3D microtissues," *Proc. Nat. Acad. Sci.*, vol. 106, no. 25, pp. 10097–10102, 2009, doi: [10.1073/pnas.0900174106](https://doi.org/10.1073/pnas.0900174106).
- [5] M. N. Hirt, A. Hansen, and T. Eschenhagen, "Cardiac tissue engineering: State of the art," *Circulation Res.*, vol. 114, no. 2, pp. 354–367, Jan. 2014, doi: [10.1161/circresaha.114.300522](https://doi.org/10.1161/circresaha.114.300522).
- [6] S. S. Nunes et al., "Biowire: A platform for maturation of human pluripotent stem cell-derived cardiomyocytes," *Nature Methods*, vol. 10, no. 8, pp. 781–787, Aug. 2013, doi: [10.1038/nmeth.2524](https://doi.org/10.1038/nmeth.2524).
- [7] J. Schwan and S. G. Campbell, "Prospects for in vitro myofilament maturation in stem cell-derived cardiac myocytes," *Biomark Insights*, vol. 10, no. 1, pp. 91–103, 2015, doi: [10.4137/bmi.S23912](https://doi.org/10.4137/bmi.S23912).
- [8] A. Leonard et al., "Afterload promotes maturation of human induced pluripotent stem cell derived cardiomyocytes in engineered heart tissues," *J. Mol. Cell Cardiol.*, vol. 118, pp. 147–158, May 2018, doi: [10.1016/j.yjmcc.2018.03.016](https://doi.org/10.1016/j.yjmcc.2018.03.016).
- [9] X. Yang, L. Pabon, and C. E. Murry, "Engineering adolescence: Maturation of human pluripotent stem cell-derived cardiomyocytes," *Circulation Res.*, vol. 114, no. 3, pp. 511–523, 2014, doi: [10.1161/CIRCRESAHA.114.300558](https://doi.org/10.1161/CIRCRESAHA.114.300558).
- [10] J.-L. Ruan et al., "Mechanical stress promotes maturation of human myocardium from pluripotent stem cell-derived progenitors," *Stem Cells*, vol. 33, no. 7, pp. 2148–2157, 2015, doi: [10.1002/stem.2036](https://doi.org/10.1002/stem.2036).
- [11] F. Xu et al., "A microfabricated magnetic actuation device for mechanical conditioning of arrays of 3D microtissues," *Lab. Chip*, vol. 15, no. 11, pp. 2496–2503, 2015, doi: [10.1039/C4LC01395F](https://doi.org/10.1039/C4LC01395F).
- [12] C. Fink et al., "Chronic stretch of engineered heart tissue induces hypertrophy and functional improvement," *FASEB J.*, vol. 14, no. 5, pp. 669–679, Apr. 2000, doi: [10.1096/fasebj.14.5.669](https://doi.org/10.1096/fasebj.14.5.669).
- [13] A. Mihic et al., "The effect of cyclic stretch on maturation and 3D tissue formation of human embryonic stem cell-derived cardiomyocytes," *Biomaterials*, vol. 35, no. 9, pp. 2798–2808, Mar. 2014, doi: [10.1016/j.biomaterials.2013.12.052](https://doi.org/10.1016/j.biomaterials.2013.12.052).
- [14] S.-J. Gwak et al., "The effect of cyclic strain on embryonic stem cell-derived cardiomyocytes," *Biomaterials*, vol. 29, no. 7, pp. 844–856, Mar. 2008, doi: [10.1016/j.biomaterials.2007.10.050](https://doi.org/10.1016/j.biomaterials.2007.10.050).
- [15] I. Mannhardt et al., "Piezo-bending actuators for isometric or auxotonic contraction analysis of engineered heart tissue," *J. Tissue Eng. Regen. Med.*, vol. 13, no. 1, pp. 3–11, Jan. 2019, doi: [10.1002/term.2755](https://doi.org/10.1002/term.2755).
- [16] A. K. Schroer et al., "I-wire heart-on-a-chip II: Biomechanical analysis of contractile, three-dimensional cardiomyocyte tissue constructs," *Acta Biomater.*, vol. 48, pp. 79–87, Jan. 2017, doi: [10.1016/j.actbio.2016.11.010](https://doi.org/10.1016/j.actbio.2016.11.010).
- [17] V. Y. Sidorov et al., "I-wire heart-on-a-chip I: Three-dimensional cardiac tissue constructs for physiology and pharmacology," *Acta Biomater.*, vol. 48, pp. 68–78, Jan. 2017, doi: [10.1016/j.actbio.2016.11.009](https://doi.org/10.1016/j.actbio.2016.11.009).
- [18] X. Lian et al., "Directed cardiomyocyte differentiation from human pluripotent stem cells by modulating Wnt/ β -catenin signaling under fully defined conditions," *Nature Protoc.*, vol. 8, no. 1, pp. 162–175, Jan. 2013, doi: [10.1038/nprot.2012.150](https://doi.org/10.1038/nprot.2012.150).
- [19] J. L. Ruan et al., "Mechanical stress conditioning and electrical stimulation promote contractility and force maturation of induced pluripotent stem cell-derived human cardiac tissue," *Circulation*, vol. 134, no. 20, pp. 1557–1567, Nov. 2016, doi: [10.1161/circulationaha.114.014998](https://doi.org/10.1161/circulationaha.114.014998).
- [20] W. J. d. Lange et al., "Human iPSC-engineered cardiac tissue platform faithfully models important cardiac physiology," *Amer. J. Physiol. Heart Circulatory Physiol.*, vol. 320, no. 4, pp. H1670–H1686, 2021, doi: [10.1152/ajpheart.00941.2020](https://doi.org/10.1152/ajpheart.00941.2020).
- [21] I. Goldfracht et al., "Engineered heart tissue models from hiPSC-derived cardiomyocytes and cardiac ECM for disease modeling and drug testing applications," *Acta Biomater.*, vol. 92, pp. 145–159, Jul. 2019, doi: [10.1016/j.actbio.2019.05.016](https://doi.org/10.1016/j.actbio.2019.05.016).
- [22] T. Boudou et al., "A microfabricated platform to measure and manipulate the mechanics of engineered cardiac microtissues," *Tissue Eng. Part A*, vol. 18, no. 9/10, pp. 910–919, May 2012, doi: [10.1089/ten.tea.2011.0341](https://doi.org/10.1089/ten.tea.2011.0341).
- [23] C. Ruwhof and A. van der Laarse, "Mechanical stress-induced cardiac hypertrophy: Mechanisms and signal transduction pathways," *Cardiovasc. Res.*, vol. 47, no. 1, pp. 23–37, 2000, doi: [10.1016/s0008-6363\(00\)00076-6](https://doi.org/10.1016/s0008-6363(00)00076-6).